

Wave mechanics and the Zeldovich approximation

C J Short and P Coles

School of Physics and Astronomy, University of Nottingham, University Park,
Nottingham, UK, NG7 2RD

E-mail: ppxcjs@nottingham.ac.uk, peter.coles@nottingham.ac.uk

Abstract. The equations of motion of a self-gravitating fluid of collisionless cold dark matter (CDM) particles can be written in the form of a Schrödinger equation coupled to a Poisson equation describing Newtonian gravity. In a spatially flat CDM-dominated universe the Schrödinger equation can be reduced to the free-particle Schrödinger equation and, in an appropriate limit, we show that the free-particle Schrödinger equation can be thought of as a wave-mechanical analogue of the Zeldovich approximation. We use the free-particle Schrödinger equation to formulate an alternative approximation method (the free-particle approximation) that is capable of following the gravitational collapse of density fluctuations into the quasi-linear regime. The free-particle approximation is tested by appealing to a cosmological N -body simulation and results are compared with the results obtained from two established approaches: linear perturbation theory and the Zeldovich-Bernoulli approximation. We find that the free-particle approximation comprehensively out-performs both of these approximation schemes in all tests carried out and thus provides another useful analytical tool for studying structure formation on cosmological scales.

PACS numbers: 95.35.+d, 98.65.Dx, 98.80.-k

Submitted to: *J. Cosmol. Astropart. Phys.*

1. Introduction

Over the last two decades a vigorous interplay between theory and observation has led to the establishment of a standard cosmological model that not only describes the composition and evolution of the universe as a whole, but has also scored great successes in accounting for the details of cosmological structure formation; for a recent review see, for example, Coles (2005). In this standard model, large-scale structure is thought to be the result of the gravitational amplification of small density perturbations present in the early universe; a mechanism known as gravitational instability. The gravitational instability process is relatively easy to understand at a qualitative level because it mostly relies only on the action of gravity with more complex hydrodynamical and radiative effects playing a role only at late times when structure is already largely developed. Moreover, when the density fluctuations are very much smaller than the average density,

the growth of fluctuations can be handled quite accurately using first-order (linear) perturbation techniques (e.g. Peebles 1980). On the other hand, galaxies and galaxy clusters represent density enhancements well in excess of the mean density so we need to go well beyond linear theory if we are to study the formation of such objects in detail.

The non-linear regime of gravitational instability is analytically intractable, except in a few cases where some special symmetry applies. For the most part, therefore, cosmologists have been forced to resort to numerical methods based on N -body computations in order to study the late stages of the evolution of density fluctuations. The use of computer simulations has revolutionized cosmology, especially in enabling the simulation of the large-scale structure expected to be found in galaxy redshift surveys and the consequent testing of models using observations. In some cases, however, such as when a very large volume and/or very high resolution is needed, one has to make more detailed predictions than can be obtained by using computational techniques. In such cases numerous analytical approximations have been suggested that provide robust results in a necessarily limited range of circumstances (e.g. Sahni and Coles 1995). These approximate techniques also help to promote a genuine understanding of the principal processes involved in the formation of cosmological structure. An important example is the Zeldovich approximation (Zeldovich 1970). This simple approximation describes important aspects of the development of the ‘cosmic web’ of filaments and voids that comprises the morphology of the large-scale galaxy distribution. The Zeldovich approximation is essentially a *kinematic* approach in which initial fluctuations in the gravitational potential induce ballistic motion of the fluid elements. This approximation is remarkably successful in describing the pattern of structure formed from realistic (random) initial conditions (Coles *et al* 1993), as long as care is taken to ensure that particle trajectories do not intersect. If trajectories cross (a phenomenon known as *shell-crossing*), the density field becomes singular and, afterwards, the approximation is hopelessly unreliable.

In this paper we approach the Zeldovich approximation from a radically new perspective, based on the description of cosmological perturbations not as particles but as waves. Inspired by Widrow and Kaiser (1993), we employ a representation of the fluid equations of motion in which the dynamics are governed by a Schrödinger equation coupled to a Poisson equation describing the action of gravity. As pointed out by Coles (2002), this approach has numerous advantages for analytical studies of gravitational instability, including the fact that it guarantees a positive-definite density field (something the usual perturbative approaches do not do). Moreover, the fuzzy nature of the description implied by quantum mechanics means that shell-crossing events do not lead to the generation of singularities. Building on a study by Coles and Spencer (2003), Short and Coles (2006) studied the behaviour of perturbative solutions of the Schrödinger equation for simple one-dimensional examples of gravitational collapse. Out of this study has emerged the realization that the free-particle limit of the Schrödinger equation bears many resemblances to the Zeldovich approximation, but also many advantages over it.

In this paper we examine the relationship between the free-particle Schrödinger equation and the Zeldovich approximation, and test the resulting approximation scheme for realistic initial conditions using N -body simulations. The layout of the paper is as follows: In section 2, we review the basics of standard (Eulerian) fluid perturbation theory, the Zeldovich approximation, the wave-mechanical approach in general, and the free-particle version in particular; see also Short and Coles (2006). The essentials of the practical implementation of this approach are discussed in section 3. In section 4 we describe the results of our comparison of the free-particle wave-mechanical approach with an N -body simulation and also assess the performance of our method relative to two standard approaches: linear perturbation theory and the Zeldovich-Bernoulli approximation. We draw our conclusions in section 5.

2. Cosmological structure formation

The Big Bang model is founded upon the Cosmological Principle, a symmetry principle that requires the universe on large scales to be both homogeneous and isotropic. Space-times consistent with this requirement are described by the Robertson–Walker metric

$$ds^2 = c^2 dt^2 - a^2 \left(\frac{dr^2}{1 - \kappa r^2} + r^2 d\theta^2 + r^2 \sin^2 \theta d\phi^2 \right), \quad (1)$$

where c is the speed of light and κ is the spatial curvature, scaled so as to take the values 0 or ± 1 . The case $\kappa = 0$ represents flat space sections, and the other two cases describe space sections of constant positive or negative curvature, respectively. The time coordinate t is *cosmological proper time* and it is singled out as a preferred time coordinate by the property of spatial homogeneity. The quantity $a = a(t)$ is the *cosmological scale factor*, describing the overall expansion of the universe as a function of proper time. The spatial coordinates (r, θ, ϕ) are comoving spherical polar coordinates.

The dynamics of a universe described by the metric (1) are governed by the Friedmann equations:

$$H^2 = \frac{8\pi G}{3} \rho_b - \frac{\kappa c^2}{a^2} + \frac{\Lambda}{3}, \quad (2)$$

$$\frac{\ddot{a}}{a} = -\frac{4\pi G}{3} \left(\rho_b + \frac{3P_b}{c^2} \right) + \frac{\Lambda}{3}, \quad (3)$$

$$\dot{\rho}_b = -3H \left(\rho_b + \frac{P_b}{c^2} \right), \quad (4)$$

where Λ is the *cosmological constant* and $H = H(t)$ is the Hubble parameter, defined by $H \equiv \dot{a}/a$. Dots are used throughout to denote a derivative with respect to proper time. The quantities $\rho_b = \rho_b(t)$ and $P_b = P_b(t)$ are the total density and pressure of the constituents of the universe, respectively. The Friedmann equations determine the time evolution of the scale factor a and therefore describe the global expansion or contraction of the universe.

The study of structure formation on cosmological scales requires an understanding of how small amplitude initial perturbations about the homogeneous and isotropic background cosmology evolve with time. In general, the evolution equations for the perturbations are obtained by applying perturbation theory to the Einstein field equations of general relativity; see, for example: Lifshitz (1946), Hawking (1966), Bardeen (1980), Kodama and Sasaki (1984, 1987), Bruni *et al* (1992), Mukhanov *et al* (1992). However, a significant simplification can be made by assuming that the length scale of the perturbations is much smaller than the Hubble radius. In this case the equations of motion for the perturbations reduce to those of Newtonian gravity (e.g. Peebles 1980). Throughout this paper we will assume that the distributions of baryonic matter, neutrinos and photons are unperturbed so that the formation of large-scale structure is a result of the gravitational amplification of primordial fluctuations in the cold dark matter (CDM) distribution only.

2.1. The fluid approach

In the Newtonian limit, the equations of motion governing the dynamics of a self-gravitating fluid of collisionless (i.e. pressureless) CDM particles can be written in the form

$$\frac{\partial \mathbf{U}}{\partial a} + (\mathbf{U} \cdot \nabla_{\mathbf{x}}) \mathbf{U} + \left(\frac{2}{a} + \frac{\ddot{a}}{a^2} \right) \mathbf{U} + \nabla_{\mathbf{x}} \Theta = 0, \quad (5)$$

$$\frac{\partial \delta}{\partial a} + \nabla_{\mathbf{x}} \cdot [(1 + \delta) \mathbf{U}] = 0, \quad (6)$$

$$\nabla_{\mathbf{x}}^2 \Theta - \frac{3\Omega_d}{2a^2} \delta = 0. \quad (7)$$

The scale factor has been normalized so that at the present epoch $a = a_0 = 1$. The spatial coordinates $\mathbf{x} = \mathbf{x}(a)$ are comoving coordinates, related to physical coordinates \mathbf{r} via $\mathbf{r} = a\mathbf{x}$. The comoving velocity field $\mathbf{U} = \mathbf{U}(\mathbf{x}, a)$ is defined by $\mathbf{U} = d\mathbf{x}/da$ and is related to the peculiar velocity field $\mathbf{v}_p = \mathbf{v}_p(\mathbf{x}, a)$ by $\mathbf{v}_p = a\dot{a}\mathbf{U}$. The field $\Theta = \Theta(\mathbf{x}, a)$ is obtained from the peculiar Newtonian gravitational potential $\Phi_p = \Phi_p(\mathbf{x}, a)$ via a simple rescaling: $\Theta = \Phi_p/a^2\dot{a}^2$. The density contrast $\delta = \delta(\mathbf{x}, a)$ is of the form $\delta = \rho/\rho_{b,d} - 1$ where $\rho = \rho(\mathbf{x}, a)$ is the CDM density field and $\rho_{b,d} = \rho_{b,d}(a)$ is the CDM density in the homogeneous background. Finally, $\Omega_d = \Omega_d(a)$ is the CDM density parameter given by $\Omega_d = 8\pi G\rho_{b,d}/3H^2$.

The system of coupled fluid equations describe how perturbations in the CDM distribution evolve with time relative to the homogeneous and isotropic background cosmological model. The fluid equations require the existence of a unique fluid velocity at every point in space. However, gravitational evolution generically leads to the formation of regions (known as *caustics*) where the trajectories of several fluid elements cross. There is typically a range of fluid velocities through a point where shell-crossing has occurred (a phenomenon known as *multi-streaming*). Consequently the velocity field

is no longer single-valued in such regions and the fluid equations cannot be applied. A more general treatment capable of handling multi-stream regions would require a solution of the collisionless Boltzmann (i.e. Vlasov) equation for the full phase-space distribution function of the system.

2.2. Linear perturbation theory

In the standard picture of cosmological structure formation the initial CDM distribution is almost homogeneous except for the presence of small fluctuations ($\delta \ll 1$) of primordial origin. The subsequent growth of these fluctuations can be followed at early times by using the linearized versions of the fluid equations. The fluid equations are linearized by perturbing \mathbf{U} , δ and Θ about their values in the background cosmology and keeping only first order terms. From the resulting linearized Euler, continuity and Poisson equations it is straightforward to obtain the following second order PDE:

$$\frac{\partial^2 \delta}{\partial a^2} + \left(\frac{2}{a} + \frac{\ddot{a}}{\dot{a}^2} \right) \frac{\partial \delta}{\partial a} - \frac{3\Omega_d}{2a^2} \delta = 0. \quad (8)$$

This equation describes how fluctuations in the CDM density field evolve with time in the linear regime. The general solution to (8) is of the form

$$\delta = AD_+ + BD_-, \quad (9)$$

where $A = A(\mathbf{x})$, $B = B(\mathbf{x})$ are functions to be determined and $D_+ = D_+(a)$, $D_- = D_-(a)$ are the so-called linear growth and decay factors respectively. It is customary to ignore the decaying mode as it is only the growing mode that is responsible for the formation of cosmic structure. If the decaying mode is neglected then the linearized continuity equation can be inverted to yield the relation

$$\delta = -\frac{a}{f} \nabla_{\mathbf{x}} \cdot \mathbf{U}, \quad (10)$$

where the function $f = f(a)$ is given by

$$f = \frac{a}{D_+} \frac{dD_+}{da}. \quad (11)$$

Inserting (10) into the linearized Poisson equation gives the following expression for the comoving velocity \mathbf{U} :

$$\mathbf{U} = -\frac{2af}{3\Omega_d} \nabla_{\mathbf{x}} \Theta + \mathbf{C}, \quad (12)$$

where $\mathbf{C} = \mathbf{C}(\mathbf{x}, a)$ is a function to be determined and $\nabla_{\mathbf{x}} \cdot \mathbf{C} = 0$. It is clear from (12) that, in the linear regime, the velocity flow associated with the growing mode is irrotational and can be written in the form $\mathbf{U} = -\nabla_{\mathbf{x}} \phi$ where $\phi = \phi(\mathbf{x}, a)$ is the comoving velocity potential given by

$$\phi = \frac{2af}{3\Omega_d} \Theta. \quad (13)$$

In the special case of a spatially-flat CDM-dominated universe (i.e. $\Omega_d = 1$) the growth and decay factors of the linear density field are $D_+ = a/a_i$ and $D_- = (a/a_i)^{-3/2}$ respectively, where a_i is some initial value of the scale factor. The function $f \equiv 1$ in this case.

2.3. The Zeldovich approximation

The Zeldovich approximation (Zeldovich 1970) provides a simple means of following the evolution of cosmic structure into the quasi-linear regime $\delta \sim 1$. The Zeldovich approximation differs from the linearized fluid approach of the previous section in the sense that it follows perturbations in particle trajectories rather than in the density field. The Zeldovich approximation has the form:

$$\mathbf{x} = \mathbf{q} + D_+ \mathbf{s}, \quad (14)$$

where $\mathbf{x} = \mathbf{x}(\mathbf{q}, t)$ is the comoving Eulerian coordinate at time t of a particle labelled by a comoving Lagrangian coordinate \mathbf{q} . The function D_+ is simply the linear growth factor introduced earlier. The vector field $\mathbf{s} = \mathbf{s}(\mathbf{q})$ is independent of time and is related to the initial velocity perturbation. The Zeldovich ansatz defines a unique mapping between the coordinates \mathbf{q} and \mathbf{x} as long as particle trajectories do not cross. The approximation breaks down when particle trajectories cross and caustics are formed as the mapping (14) is no longer unique. The density becomes formally infinite in regions where shell-crossing has occurred.

The Zeldovich approximation has been extensively tested (Coles *et al* 1993) and has been found to consistently give more accurate results than linear perturbation theory (LPT), even in the linear regime. The success of the Zeldovich approximation in the quasi-linear regime is usually attributed to the fact that the density contrast in the Zeldovich approximation is intrinsically a non-linear function of the displacement $\mathbf{x} - \mathbf{q}$. Also, the accuracy of the Zeldovich approximation improves as the dimensionality of the collapse decreases and is in fact exact in one-dimension up until shell-crossing occurs. This is a convenient property of the Zeldovich approximation since the gravitational collapse of a density perturbation tends to proceed preferentially along the direction of the strongest gravitational force thus becoming progressively lower dimensional as time passes. For a discussion of this feature of the Zeldovich approximation, see Yoshisato *et al* (2006).

2.4. The Zeldovich-Bernoulli approximation

The Zeldovich approximation (14) can be used along with the Euler equation (under the assumption that shell-crossing has not yet occurred) to derive an Eulerian representation of the Zeldovich approximation (Nusser and Dekel 1992). The resulting first-order PDE is termed the Zeldovich-Bernoulli equation and is given by

$$\frac{\partial \phi}{\partial a} + \left(\frac{2}{a} + \frac{\ddot{a}}{a^2} - \frac{3\Omega_d}{2af} \right) \phi - \frac{1}{2} |\nabla_{\mathbf{x}} \phi|^2 = 0, \quad (15)$$

where the comoving velocity potential ϕ is related to the scaled peculiar gravitational potential Θ via

$$\phi = \frac{2af}{3\Omega_d} \Theta. \quad (16)$$

The Zeldovich-Bernoulli equation can be used to evolve the initial comoving velocity potential forwards in time. At any time of interest the CDM density field is determined from ϕ by applying (16) in conjunction with the Poisson equation. It is interesting to note that the Zeldovich-Bernoulli approximation guarantees an irrotational velocity flow and that the relationship between ϕ and Θ is the same as in LPT (13). The velocity flow will in fact remain irrotational into the quasi-linear regime as a consequence of Kelvin's circulation theorem. However, in the case of a collisionless medium, Kelvin's theorem fails when shell-crossing occurs if the fluid velocity is subsequently defined as an average over the velocities of the different streams passing through the caustic. Vorticity can then be generated in collapsing regions and we can no longer assume that the velocity flow is globally irrotational; see Pichon and Bernardeau (1999) for a discussion of vorticity generation in caustics.

In the case of a spatially flat CDM-dominated universe (i.e. $\Omega_d = f = 1$) the Zeldovich-Bernoulli equation (15) reduces to

$$\frac{\partial \phi}{\partial a} - \frac{1}{2} |\nabla_{\mathbf{x}} \phi|^2 = 0. \quad (17)$$

2.5. The wave-mechanical approach

A novel approach to the study of large-scale structure formation was suggested by Widrow and Kaiser (1993). It involves rewriting the fluid equations of motion in the form of a non-linear Schrödinger equation. We have seen that the comoving velocity flow associated with the growing mode is irrotational in the linear regime. The Zeldovich-Bernoulli approximation also guarantees that the comoving velocity field is irrotational as long as shell-crossing has not yet occurred. Assuming that a comoving velocity potential ϕ can be defined, the Euler equation (5) can be integrated once to obtain the Bernoulli equation

$$\frac{\partial \phi}{\partial a} - \frac{1}{2} |\nabla_{\mathbf{x}} \phi|^2 - \mathcal{V} = 0, \quad (18)$$

where the effective potential $\mathcal{V} = \mathcal{V}(\mathbf{x}, a)$ depends on both the comoving velocity potential and the scaled peculiar gravitational potential:

$$\mathcal{V} = \Theta - \left(\frac{2}{a} + \frac{\ddot{a}}{\dot{a}^2} \right) \phi. \quad (19)$$

The Bernoulli equation (18) and the continuity equation (6) can be combined by performing a transformation of the form

$$\psi = \sqrt{(1 + \delta)} \exp \left(\frac{-i\phi}{\nu} \right) \quad (20)$$

where $\psi = \psi(\mathbf{x}, a)$ and $\nu > 0$ is an adjustable (real) parameter with dimensions of L^2 . The transformation (20) is known as the *Madelung transformation* (Madelung 1926). Applying the Madelung transformation yields the following coupled Schrödinger-Poisson system:

$$i\nu \frac{\partial \psi}{\partial a} = \left(-\frac{\nu^2}{2} \nabla_{\mathbf{x}}^2 + \mathcal{V} + \mathcal{P} \right) \psi, \quad (21)$$

$$\nabla_{\mathbf{x}}^2 \left[\mathcal{V} - \left(\frac{2}{a} + \frac{\ddot{a}}{\dot{a}^2} \right) \nu \arg(\psi) \right] - \frac{3\Omega_d}{2a^2} (|\psi|^2 - 1) = 0, \quad (22)$$

where $\mathcal{P} = \mathcal{P}(\mathbf{x}, a)$ is the so-called *quantum pressure* term given by

$$\mathcal{P} = \frac{\nu^2}{2} \frac{\nabla_{\mathbf{x}}^2 |\psi|}{|\psi|}. \quad (23)$$

The non-linear Schrödinger equation (21) describes the time-evolution of the wavefunction ψ which can be thought of as a (complex) field representing classical CDM. The wavefunction (20) encodes both density and velocity information in a single function. At any time of interest the CDM density field δ and the comoving velocity potential ϕ can be determined from the amplitude and phase of the wavefunction respectively.

The Schrödinger equation (21) looks very similar to the familiar Schrödinger equation of quantum mechanics except for the presence of the non-linear quantum pressure term \mathcal{P} . If the quantum pressure term is neglected then we are left with the linear Schrödinger equation

$$i\nu \frac{\partial \psi}{\partial a} = \left(-\frac{\nu^2}{2} \nabla_{\mathbf{x}}^2 + \mathcal{V} \right) \psi. \quad (24)$$

Inserting the Madelung form (20) for the wavefunction into (24) yields the usual continuity equation (6) and a modified Bernoulli equation of the form

$$\frac{\partial \phi}{\partial a} - \frac{1}{2} |\nabla_{\mathbf{x}} \phi|^2 - \mathcal{V} + \mathcal{P} = 0. \quad (25)$$

The Bernoulli equation now contains an extra term which resembles a pressure term. This is why \mathcal{P} is called the quantum pressure. Notice that the quantum pressure term is proportional to ν^2 and that this is the only term in the modified Bernoulli equation (25) which depends on ν . Thus, in the limit $\nu \rightarrow 0$, we might intuitively expect to recover the usual Bernoulli equation (18). The limit $\nu \rightarrow 0$ corresponds to the semi-classical (WKB) limit of the Schrödinger equation; see, for example, Sakurai (1985) for a summary of the WKB methodology. In light of this discussion we are free to drop the quantum pressure term from the non-linear Schrödinger equation (21) and include it in the Bernoulli equation instead. This is the approach that we adopt throughout this paper.

A key advantage of the wave-mechanical approach discussed above is that the CDM density field is guaranteed to be everywhere non-negative (as it should be) since, by

construction, $\delta = |\psi^2| - 1$ and $|\psi|^2 \geq 0$. This is not always the case in LPT and the Zeldovich-Bernoulli approximation which both (erroneously) predict the formation of regions with $\delta < -1$ at late times. Another way of thinking about this is that, by solving the Schrödinger equation (24), we are effectively solving a modified Bernoulli equation of the form (25) coupled to the continuity equation (6); the continuity equation ensures that matter is conserved. Also, shell-crossing does not lead to the formation of singularities in the density field as in the Zeldovich approximation since particles are not treated as point-like entities with definite trajectories. However, the wave-mechanical approach we have outlined here is not strictly valid once shell-crossing generates multi-stream regions; in particular we can no longer adopt the simple Madelung form (20) of the wavefunction. This is because the wave-mechanical approach is derived from the usual fluid equations under the assumption that the comoving velocity field is irrotational. As we have said, this assumption is not globally true once shell-crossing occurs and, more fundamentally, the underlying fluid equations themselves cannot describe multi-streaming. It is interesting to note that the wave-mechanical approach can be adapted to deal with post shell-crossing phenomena by utilising a more sophisticated representation of the wavefunction. This was done by Widrow and Kaiser (1993) who used the Husimi representation (Husimi 1940) of the wavefunction as a model of collisionless CDM. They constructed a Schrödinger distribution function and showed that this distribution function obeys an equation that reduces to the Vlasov equation in a suitable limit; see also Skodje *et al* (1989). The method they proposed was indeed found to be capable of handling multi-streaming when tested on simple examples (Widrow and Kaiser 1993, Davies and Widrow 1997).

2.6. The free-particle approximation

The coupled Schrödinger-Poisson system is valid for a general homogeneous and isotropic background cosmological model. In most cases the system must be solved numerically or via approximation methods; Short and Coles (2006) used perturbation theory to find approximate solutions of the Schrödinger equation in simple scenarios. However, as noted by Short and Coles (2006), we can make a considerable simplification by assuming that the universe is spatially-flat and dominated by CDM (i.e. $\Omega_d = 1$). In this case the linearized fluid and Zeldovich-Bernoulli approximations predict that the comoving velocity potential and the scaled peculiar gravitational potential satisfy $\phi = 2a\Theta/3$. If we assume that ϕ and Θ are related in this manner then it is clear from (19) that the effective potential \mathcal{V} is identically zero. This is an important observation as the linear Schrödinger equation (24) then reduces to the free-particle Schrödinger equation

$$i\nu \frac{\partial \psi}{\partial a} = -\frac{\nu^2}{2} \nabla_{\mathbf{x}}^2 \psi, \quad (26)$$

and the Poisson equation (22) becomes

$$\nu \nabla_{\mathbf{x}}^2 [\arg(\psi)] + \frac{1}{a} (|\psi|^2 - 1) = 0. \quad (27)$$

The free-particle Schrödinger equation has an exact analytical solution. The easiest way to construct the solution to (26) is in Fourier space; for each comoving wavevector \mathbf{k} we have that

$$\hat{\psi} = \hat{\psi}_i \exp \left[\frac{-i\nu(a - a_i)k^2}{2} \right] \quad (28)$$

where $\hat{\psi} = \hat{\psi}(\mathbf{k}, a)$, $\hat{\psi}_i = \hat{\psi}(\mathbf{k}, a_i)$ are the Fourier transforms of the wavefunction and the initial wavefunction respectively and $k = |\mathbf{k}|$.

It is interesting to note that, if the Madelung form (20) for the wavefunction is substituted into the free-particle Schrödinger equation, then we recover the Bernoulli equation (25) with $\mathcal{V} \equiv 0$. The resulting equation is very similar to the Zeldovich-Bernoulli equation (17) except for the presence of the quantum pressure term \mathcal{P} . Thus it seems as if we should regain the Zeldovich-Bernoulli equation in the limit $\nu \rightarrow 0$. It is also possible to show that in the limit $\nu \rightarrow 0$ the free-particle Schrödinger equation gives rise to Zeldovich trajectories of the form (14); see Appendix A for details. These points suggest that the free-particle Schrödinger equation can be thought of as a wave-mechanical analogue of the Zeldovich approximation. We term this alternative approximation method the free-particle approximation. The free-particle approximation has already been successfully applied to simple one-dimensional examples of gravitational collapse; see Coles and Spencer (2003) and Short and Coles (2006) for details. However, the aim of this work is to test the free-particle approximation in a more cosmologically relevant scenario.

3. Testing the free-particle approximation

In modern cosmology the process of structure formation on cosmological scales is almost exclusively studied using numerical N -body methods. In a typical N -body simulation the CDM distribution is approximated by N particles (mass tracers) of identical mass contained within a large simulation volume. The simulation volume is usually a comoving cube equipped with periodic boundary conditions and the cubic volume is chosen to be large enough that it is ‘representative’ of the universe. At the start of the simulation run the N particles are typically placed on a uniform cubic grid. The Zeldovich approximation is then used along with the (cosmology dependent) power spectrum of CDM density fluctuations to perturb the particle positions from a uniform distribution. The particles are also assigned velocities in accordance with the Zeldovich approximation. The CDM distribution is then allowed to evolve solely under the action of Newtonian gravity until the end of the simulation run is reached.

The gravitational collapse of initial density perturbations can be successfully followed well into the non-linear regime using N -body methods which is something that cannot be done with any analytical approximation. This means that N -body simulations provide an ideal tool for testing the applicability of analytical approximation methods. In this paper we test the free-particle, linearized fluid and Zeldovich-Bernoulli

approximations against an N -body simulation so that we may assess the performance of the new free-particle approximation relative to existing methods.

3.1. The N -body simulation

The adaptive P³M code HYDRA (Couchman *et al* 1995) was used to perform an N -body simulation. The simulation consisted of $N = 128^3$ CDM particles contained within a cubic box of comoving side length $L = 200h^{-1}$ Mpc equipped with periodic boundary conditions. Here h is the present value of the Hubble parameter H_0 in units of 100 km s⁻¹ Mpc⁻¹. A standard CDM cosmological model was assumed with parameters $\Omega_{\mathrm{d},0} = 1$, $\Omega_{\mathrm{b},0} = 0$, $\Omega_{\Lambda,0} = 0$, $h = 0.71$ where $\Omega_{\mathrm{d},0}$, $\Omega_{\mathrm{b},0}$ and $\Omega_{\Lambda,0}$ are the present values of the CDM, baryon and cosmological constant density parameters respectively. The simulation began at an initial redshift of $1 + z_{\mathrm{i}} = 50$ and the particles were initially positioned so as to form a random realization of a CDM density field with a power spectrum $P = P(k)$ of the form:

$$P = T^2 P_{\mathrm{i}}, \quad (29)$$

where $P_{\mathrm{i}} = P_{\mathrm{i}}(k)$ is the primordial power spectrum of density fluctuations generated by inflation and $T = T(k)$ is the *transfer function*. We assume that the primordial power spectrum is scale-invariant $P_{\mathrm{i}} \propto k$ as predicted by a general class of inflationary models; see Brandenberger (1985) for a review. The following empirical form for the CDM transfer function is adopted (Bardeen *et al* 1986):

$$T = \frac{\log(1 + 2.34q)}{2.34q} [1 + 3.89q + (16.1q)^2 + (5.46q)^3 + (6.71q)^4]^{-1/4}, \quad (30)$$

where $q = q(k)$ is given by $q = k\theta^{1/2}/\Omega_{\mathrm{d},0}h^2$ and $\theta = \kappa/1.68$. Here $\kappa = \Omega_{\mathrm{r},0}/\Omega_{\gamma,0}$ is the ratio of the present relativistic particle and photon density parameters respectively; in a universe with three relativistic neutrino flavours and photons $\kappa = 1.68$. Finally, the power spectrum was normalized so that the present value of the rms density fluctuation in spheres of radius $8h^{-1}$ Mpc ($\sigma_{8,0}$) was 0.84.

The Newtonian gravitational evolution of the CDM distribution was then followed from the initial redshift to the present $z_0 = 0$. The gravitational forces are calculated within the code on a uniform mesh with 256^3 grid points. At each time step in the simulation the N -body code stores the comoving positions and velocities of all N particles.

3.2. The testing process

To test the Eulerian free-particle, linearized fluid and Zeldovich-Bernoulli approximations against the Lagrangian N -body simulation described above, we divide the cubic simulation volume (of comoving side length $200h^{-1}$ Mpc) into a uniform cubic mesh with $N_{\mathrm{g}} = 128^3$ grid points. There is then one particle per grid cell (on average) and the comoving separation between neighbouring grid points in the mesh is

$\Delta = L/N_g^{1/3} = 1.5625h^{-1}$ Mpc which is roughly the size of a typical galaxy group. We now describe in turn how each of the approximation schemes is tested.

The free-particle approximation. The first step in testing the free-particle approximation is to construct an initial wavefunction of the form

$$\psi_i = \sqrt{(1 + \delta_i)} \exp\left(\frac{-i\phi_i}{\nu}\right) \quad (31)$$

on the cubic mesh. In order to do this we must calculate the initial CDM density field δ_i and the initial comoving velocity field \mathbf{U}_i . These fields are generated on the mesh by applying triangular-shaped cloud interpolation (e.g. Hockney and Eastwood 1988) to the initial positions and velocities of the particles in the N -body simulation, respectively. Once \mathbf{U}_i is known then the initial comoving velocity potential ϕ_i can be determined on the cubic mesh by numerically solving

$$\nabla_{\mathbf{x}}^2 \phi_i = -\nabla_{\mathbf{x}} \cdot \mathbf{U}_i \quad (32)$$

in Fourier space. The fields δ_i and ϕ_i are inserted into (31) along with a suitable value of the free parameter ν to give the desired initial wavefunction. We shall return to the question of what constitutes a suitable value of ν in section 4. The discrete Fourier transform $\hat{\psi}_i$ of the initial wavefunction is then calculated and the free-particle solution (28) is used to calculate the Fourier transform $\hat{\psi}$ of the wavefunction at any $a \geq a_i$ of interest. The wavefunction ψ in real space follows by taking the inverse discrete Fourier transform of $\hat{\psi}$. The CDM density field is determined from the amplitude of the wavefunction via $\delta = |\psi|^2 - 1$. As we shall see in section 4, knowledge of the comoving velocity potential ϕ is also useful. The comoving velocity potential can be calculated on the cubic mesh by using numerical Fourier techniques to solve the Poisson equation (27) in the form

$$\nabla_{\mathbf{x}}^2 \phi = \frac{\delta}{a}. \quad (33)$$

It is worth noting that the comoving velocity potential can also be extracted from the phase of the wavefunction directly. However, there are some subtleties involved; it is important to distinguish the difference between so-called *wrapped* and *unwrapped* phase. If we define a field $\vartheta = \vartheta(\mathbf{x}, a)$ by $\vartheta = \arg(\psi)$ then the values of ϑ are constrained to lie in the range $-\pi < \vartheta \leq \pi$; the phase is said to be wrapped into the interval $(-\pi, \pi]$. The wrapped phase field ϑ is typically discontinuous as there are phase jumps of magnitude 2π every time the phase changes from $\pm\pi$ to $\mp\pi$. In order to obtain a continuous phase field $\varphi = \varphi(\mathbf{x}, a)$ from ϑ some kind of *unwrapping* operation must be applied to the wrapped phase. Once the continuous unwrapped phase φ is known then the comoving velocity potential can be calculated via $\phi = -\nu\varphi$. Unfortunately, extracting the unwrapped phase φ from the wrapped phase ϑ is by no means a trivial task (see Ghiglia and Pritt 1998 for a comprehensive introduction to phase unwrapping); this is why we calculate the comoving velocity potential by solving the Poisson equation

(33) instead. However, in cases where the full Schrödinger-Poisson system must be solved (i.e. if we were considering a more general cosmological model), the Poisson equation would not be in the convenient form (33). In such cases the only way to extract velocity information from the wavefunction would be by unwrapping the phase of the wavefunction.

Linear perturbation theory. To test the linearized fluid approach, the initial CDM density field δ_i is first constructed on the cubic mesh in the same way as described above. The linear growth law

$$\delta = \left(\frac{a}{a_i} \right) \delta_i \quad (34)$$

is then used to determine the density field δ on the mesh for any $a \geq a_i$.

The Zeldovich-Bernoulli approximation. The initial comoving velocity potential ϕ_i is constructed on the cubic mesh as before and the Zeldovich-Bernoulli equation

$$\frac{\partial \phi}{\partial a} - \frac{1}{2} |\nabla_{\mathbf{x}} \phi|^2 = 0 \quad (35)$$

is integrated forwards in time from $a_i = 0.02$ to $a_0 = 1$ using the the simple numerical scheme described in Nusser and Dekel (1992). At each time step in the integration we know ϕ and so the CDM density field δ can be numerically calculated on the mesh via the relation

$$\delta = a \nabla_{\mathbf{x}}^2 \phi. \quad (36)$$

4. Results and discussion

It is informative to examine the behaviour of the free-particle approximation before testing the method against LPT and the Zeldovich-Bernoulli approximation. In particular it is important to investigate the effect of varying the free parameter ν and the role of the quantum pressure term \mathcal{P} . Before continuing our discussion we introduce a dimensionless parameter Γ given by

$$\Gamma = \frac{\nu}{\Delta^2}, \quad (37)$$

where $\Delta = 1.5625h^{-1}$ Mpc is the comoving separation between neighbouring grid points in the cubic mesh. The parameter Γ emerges from rewriting the free-particle Schrödinger equation (26) in terms of the dimensionless comoving coordinate $\bar{\mathbf{x}} = \mathbf{x}/\Delta$. Notice that $\Gamma \propto \nu$; hereafter we will analyse the behaviour of the free-particle approximation in terms of the value of Γ rather than ν .

4.1. Behaviour of the free-particle approximation

Figure 1 shows point-by-point comparisons of the free-particle density field δ_{fp} and the N -body density field δ_{nb} at three different values of the scale factor and for three different choices of the parameter Γ . Overlaid on each plot is the diagonal line $\ln(2 + \delta_{\text{fp}}) = \ln(2 + \delta_{\text{nb}})$; if the free-particle density field matched the N -body density field at all points in the cubic mesh then there would be zero scatter about this line. We quantify any scatter about the diagonal by using the correlation coefficient

$$r_\delta = \frac{\langle \delta_{\text{fp}} \delta_{\text{nb}} \rangle}{\langle \delta_{\text{fp}}^2 \rangle^{1/2} \langle \delta_{\text{nb}}^2 \rangle^{1/2}}; \quad (38)$$

a value of $r_\delta = 1$ corresponds to the case where there is no scatter. The main purpose of figure 1 is to illustrate the effect of varying the parameter Γ on the the free-particle approximation. The first column of figure 1 shows point-by-point comparisons of the free-particle and N -body density fields for the case when $\Gamma = 4.5$. As the scale factor increases, the agreement between the two density fields gets worse in the sense that the scatter about the diagonal grows and the value of r_δ decreases. At late times the N -body density field is extremely non-linear with large over-densities $\delta \sim 100$ present. The free-particle density field appears to deviate most from the N -body density field in these high density regions. This is to be expected as the assumptions used to construct the free-particle approximation are only valid up until shell-crossing occurs and so it is not surprising that it does not perform well in highly non-linear collapsing regions. In the case where $\Gamma = 20$ (the second column of figure 1) the performance of the free-particle approximation relative to the N -body simulation is consistently worse than in the $\Gamma = 4.5$ case. In particular, fluctuations in the free-particle density field grow at a much lesser rate. Consequently a larger discrepancy between the free-particle and N -body density fields develops as the scale factor increases. Again this is particularly true in high density regions of the N -body density field. The third column of figure 1 compares the density field obtained from the free-particle approximation with $\Gamma = 500$ to the N -body density field. In this case there is no growth of density fluctuations in the free-particle approximation. In fact, the free-particle density field oscillates in a seemingly random fashion as the scale factor increases and no large-scale structure is formed. This is why the agreement between the free-particle and N -body density fields is so poor in this case.

The effect of varying the parameter Γ in the free-particle approximation can also be clearly seen by inspecting the free-particle density field visually. Figure 2 shows slices through the present (i.e. at $a_0 = 1$) N -body and free-particle density fields for the cases $\Gamma = 4.5$, $\Gamma = 20$ and $\Gamma = 500$. The global morphology of the free-particle density field seems to match that of the N -body density field in the $\Gamma = 4.5$ case. In particular, the peaks of the N -body and free-particle density fields are located at the same positions. However, the over-densities formed in the free-particle approximation are not as large as in the N -body simulation and the free-particle density field is considerably smoother than the N -body density field. As the value of Γ is increased to 20, the free-particle

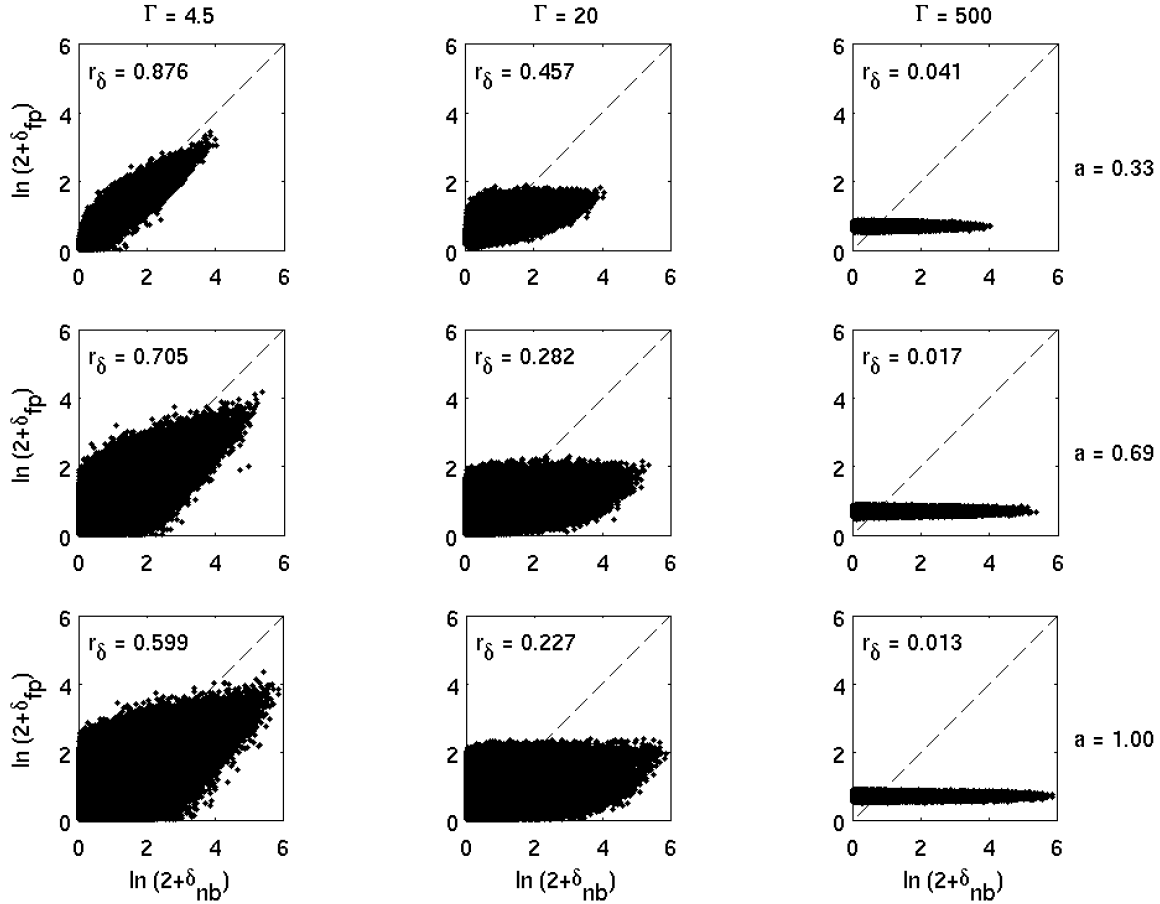


Figure 1. Point-by-point comparisons of the free-particle density field δ_{fp} and the N -body density field δ_{nb} . Comparisons are shown for three different values of the scale factor a and for three choices of the dimensionless parameter Γ . A logarithmic scale is used to make the effect of varying Γ clear. The corresponding value of the correlation coefficient r_δ between the two density fields is shown in the top-left corner of each plot.

density field appears more heavily smoothed. However, the correspondence between the location of the peaks in the free-particle and N -body density fields seems to be preserved. In the case where $\Gamma = 500$ the overall morphology of the free-particle density field is completely different to that of the N -body density field. Specifically, the free-particle density field is much more homogeneous and there is no large-scale structure. There is small-scale structure present in the free-particle density field but this structure is transient and changes rapidly with time.

In light of the previous remarks it is evident that the free-particle method performs increasingly poorly relative to the N -body simulation as the value of Γ is made larger. More specifically, as Γ is increased, the growth of density fluctuations in the free-particle approximation appears to be impeded in some way; for large enough values of Γ there is no growth of large-scale structure at all. We believe that the quantum pressure term \mathcal{P} is responsible for this effect. Recall that the free-particle Schrödinger equation (26)

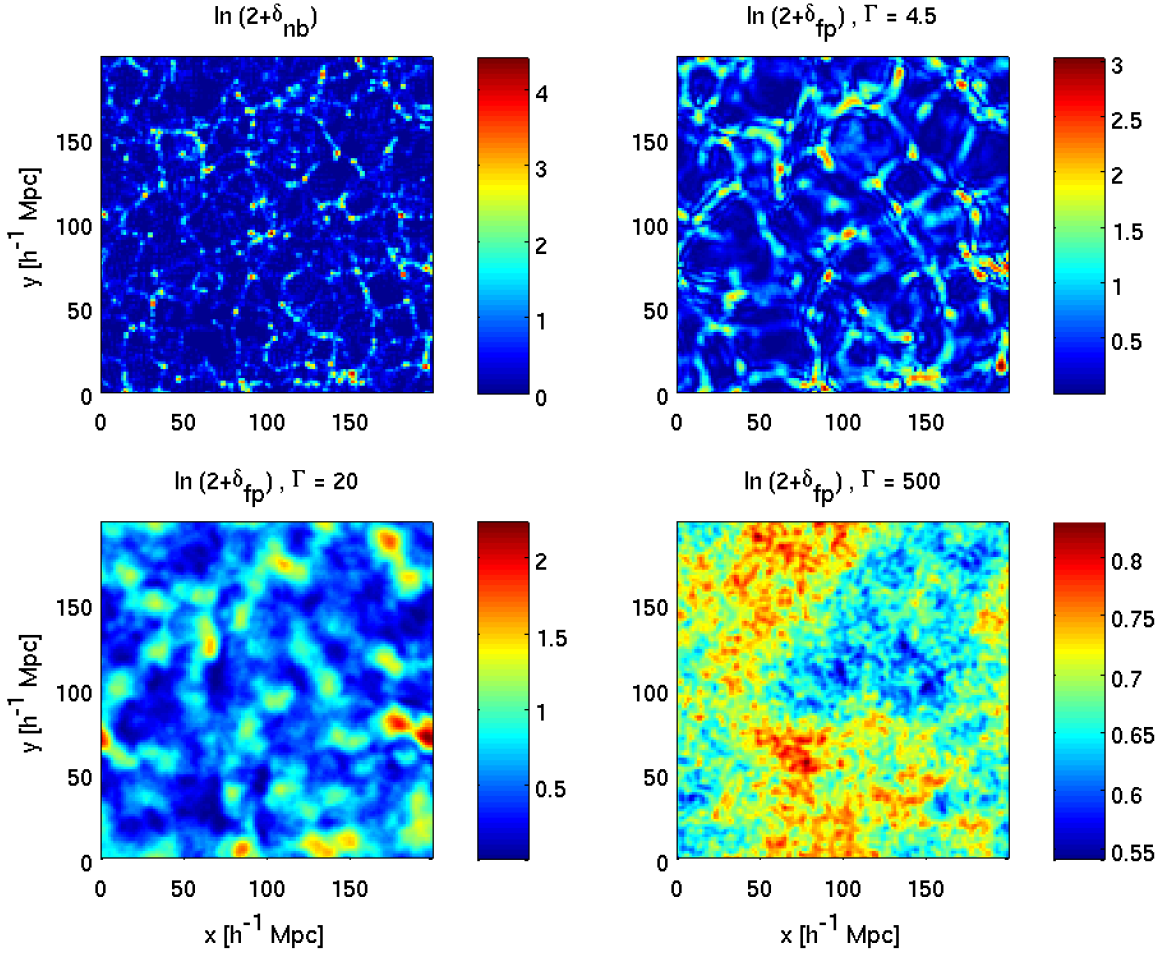


Figure 2. Slices through the N -body density field δ_{nb} and the free-particle density fields δ_{fp} for three different choices of the dimensionless parameter Γ . The value of the scale factor is $a = a_0 = 1$ and the slices are arbitrarily taken at a z -coordinate of $100h^{-1}$ Mpc. A logarithmic scale is used for clarity.

yields a modified Bernoulli equation of the form

$$\frac{\partial \phi}{\partial a} + \mathcal{C} + \mathcal{P} = 0 \quad (39)$$

upon applying the Madelung transformation (20). Here $\mathcal{C} = \mathcal{C}(\mathbf{x}, a)$ is the *convective* term, defined by

$$\mathcal{C} = -\frac{1}{2} |\nabla_{\mathbf{x}} \phi|^2, \quad (40)$$

and \mathcal{P} is the quantum pressure term:

$$\mathcal{P} = \frac{\nu^2}{2} \frac{\nabla_{\mathbf{x}}^2 \sqrt{(1 + \delta)}}{\sqrt{(1 + \delta)}}. \quad (41)$$

The definition of the parameter Γ implies that $\mathcal{P} \propto \Gamma^2$ and so, by inspecting (39), we expect Γ to control the relative contributions of the quantum pressure and convective

terms to the gravitational dynamics. To investigate this we compare the mean of the magnitude of the quantum pressure term with the mean of the magnitude of the convective term by introducing a ratio $\chi = \chi(a)$ defined by

$$\chi = \frac{\langle |\mathcal{P}| \rangle}{\langle |\mathcal{C}| \rangle}. \quad (42)$$

Figure 3 illustrates how χ evolves with time. For the moment we focus our attention on the three solid lines shown in figure 3; these lines correspond to the values $\Gamma = 4.5$, $\Gamma = 20$ and $\Gamma = 500$ respectively. It is clear that the ratio χ increases monotonically with time in all cases. This signifies that, on average, the quantum pressure becomes more important relative to the convective term as time proceeds. However, the most important point to note from figure 3 is that, at any particular value of the scale factor, the value of χ increases as Γ is increased. This means that, on average, the quantum pressure term becomes more significant (relative to the convective term) as the value of Γ is made larger. In fact, if Γ is chosen to be large enough (e.g. $\Gamma = 500$) then the quantum pressure term completely dominates the convective term in (39). As we have seen, the performance of the free-particle approximation worsens as Γ is increased and so it seems that this is indeed due to the quantum pressure term. The quantum pressure term appears to inhibit the growth of density perturbations in the free-particle approximation in some way. This behaviour was also observed in the simple tests of the free-particle approximation performed by Short and Coles (2006). In their work it was noted that gas pressure in a baryonic fluid causes a qualitatively similar effect but caution must be exercised in directly comparing the effects of quantum and classical pressure terms since the origin and form of these two terms is very different.

The above comments regarding the quantum pressure term suggest that we can minimize the effect of this term by choosing the value of Γ to be as small as possible. In the limit $\Gamma \rightarrow 0$ we expect the quantum pressure term to be completely dominated by the convective term in (39). Recall that it is in the limit $\Gamma \rightarrow 0$ (i.e. $\nu \rightarrow 0$) that the free-particle Schrödinger equation can be thought of as a wave-mechanical analogue of the Zeldovich approximation. However, in practice, we cannot choose the value of Γ to be arbitrarily small. The phase φ_i of the initial wavefunction is given by $\varphi_i = -\phi_i/\nu$ and so $\varphi_i \propto 1/\Gamma$. Thus, in the limit $\Gamma \rightarrow 0$, the phase φ_i varies increasingly rapidly and regions develop in the phase field where the magnitude of the phase change between neighbouring points in the mesh (i.e. points separated by a distance Δ) exceeds π radians. On the other hand, sampling at the Nyquist rate (the minimum possible sampling rate) is equivalent to requiring that the magnitude of the phase change over a distance Δ must be less than or equal to π radians. This means that as $\Gamma \rightarrow 0$ the initial phase field φ_i becomes insufficiently sampled and so-called phase-aliasing occurs. Typically we find that there is some critical value Γ_c of the parameter Γ such that phase-aliasing occurs if $0 < \Gamma < \Gamma_c$. If the value of Γ used in the free-particle approximation is less than Γ_c then phase-aliasing effects cause the power spectrum of the initial wavefunction ψ_i to be very noisy and the free-particle approximation breaks

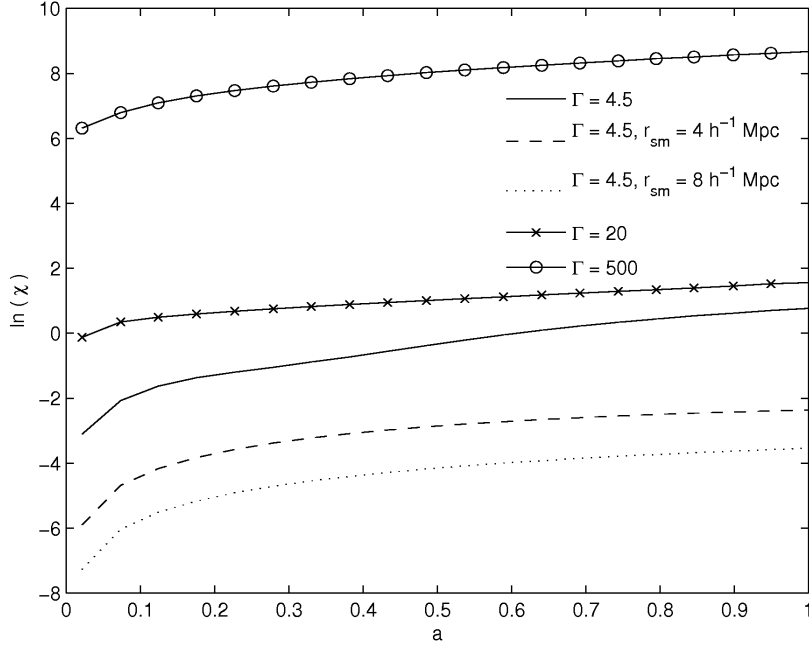


Figure 3. The ratio $\chi = \langle |\mathcal{P}| \rangle / \langle |\mathcal{C}| \rangle$ plotted as a function of the scale factor a for three different values of the parameter Γ . The dashed and dotted lines show how χ evolves when the free-particle density field and comoving velocity potential (with $\Gamma = 4.5$) have been smoothed with Gaussian filters of radius $r_{\text{sm}} = 4h^{-1}$ Mpc and $r_{\text{sm}} = 8h^{-1}$ Mpc respectively. A logarithmic scale is used for clarity.

down. Therefore, Γ_c is the smallest value of Γ that can be used in the free-particle approximation in practice. The value of Γ_c can be found by using a simple numerical algorithm; in the work presented here $\Gamma_c = 4.5$. In the remainder of our discussion we set $\Gamma = \Gamma_c = 4.5$ in the free-particle approximation. This ensures that the effect of the quantum pressure term is kept to a minimum and so the free-particle approximation will give the best possible results for the particular grid geometry we are considering.

4.2. Comparison of approximation schemes

We now use the method described in section 3.2 to test the free-particle approximation (with $\Gamma = 4.5$) against LPT and the Zeldovich-Bernoulli approximation. Figure 4 shows point-by-point comparisons of the density fields obtained from the three approximation methods with the N -body density field. The first, second and third columns correspond to the free-particle approximation, the linearized fluid approach and the Zeldovich-Bernoulli approximation respectively. Comparisons are shown for three different values of the scale factor. All of the density fields have been smoothed with a Gaussian filter of radius $r_{\text{sm}} = 4h^{-1}$ Mpc. We apply a filter to the density fields in order to smooth over highly non-linear regions where the linear/quasi-linear approximation methods cannot be expected to give reliable results.

The main result of figure 4 is that the free-particle approximation performs significantly better than both the Zeldovich-Bernoulli approximation and LPT when

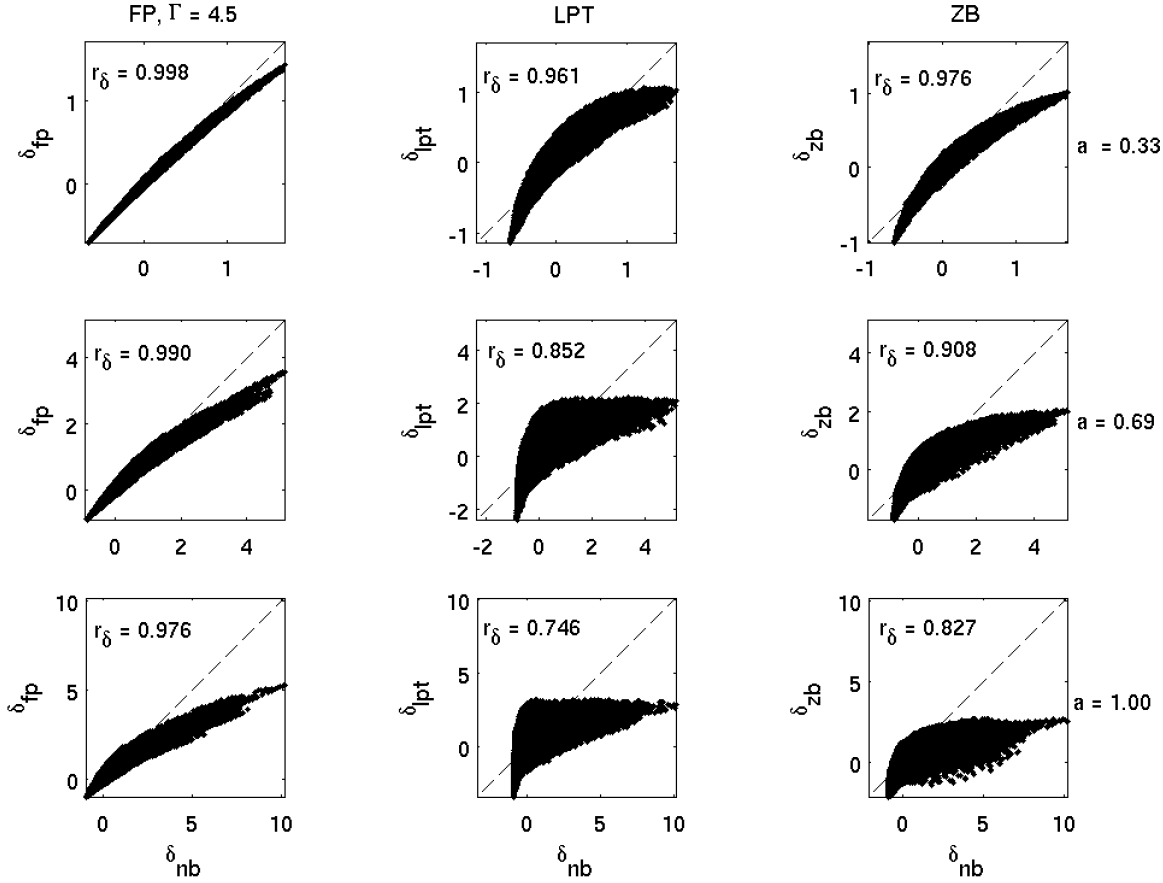


Figure 4. Point-by-point comparisons of the density fields obtained from the three approximation schemes and the N -body density field δ_{nb} . The first, second and third columns correspond to the free-particle (with $\Gamma = 4.5$), linearized fluid and Zeldovich-Bernoulli approximations respectively. Comparisons are shown for three different values of the scale factor a and all of the density fields have been smoothed with a Gaussian filter of radius $r_{\text{sm}} = 4h^{-1}$ Mpc. The corresponding value of the correlation coefficient r_δ between the density fields is shown in the top-left corner of each plot.

tested against an N -body simulation. It is clear from the point-by-point comparisons that, at any given value of the scale factor, the free-particle density field shows the best correlation with the N -body density field. Notice that the linearized fluid approach and the Zeldovich-Bernoulli approximation predict the formation of unphysical regions in the density field where $\delta < -1$, i.e. where $\rho < 0$. This problem is completely avoided in the free-particle approximation since, by definition, $\delta = |\psi|^2 - 1$ and $|\psi|^2 \geq 0$. This explains why the free-particle density field matches the N -body density field in low density regions better than the linearized fluid and Zeldovich-Bernoulli density fields. It is evident from figure 4 that all of the approximation methods systematically underestimate the density in high density regions of the smoothed N -body density field. This is not surprising as the density contrast in such regions is typically $\delta \sim 10$ and the approximation methods we are testing are designed to operate in the linear/quasi-linear regime $\delta \sim 1$. However, it is interesting to note that the free-particle approximation seems to perform better

than the other approximation methods in high density regions too.

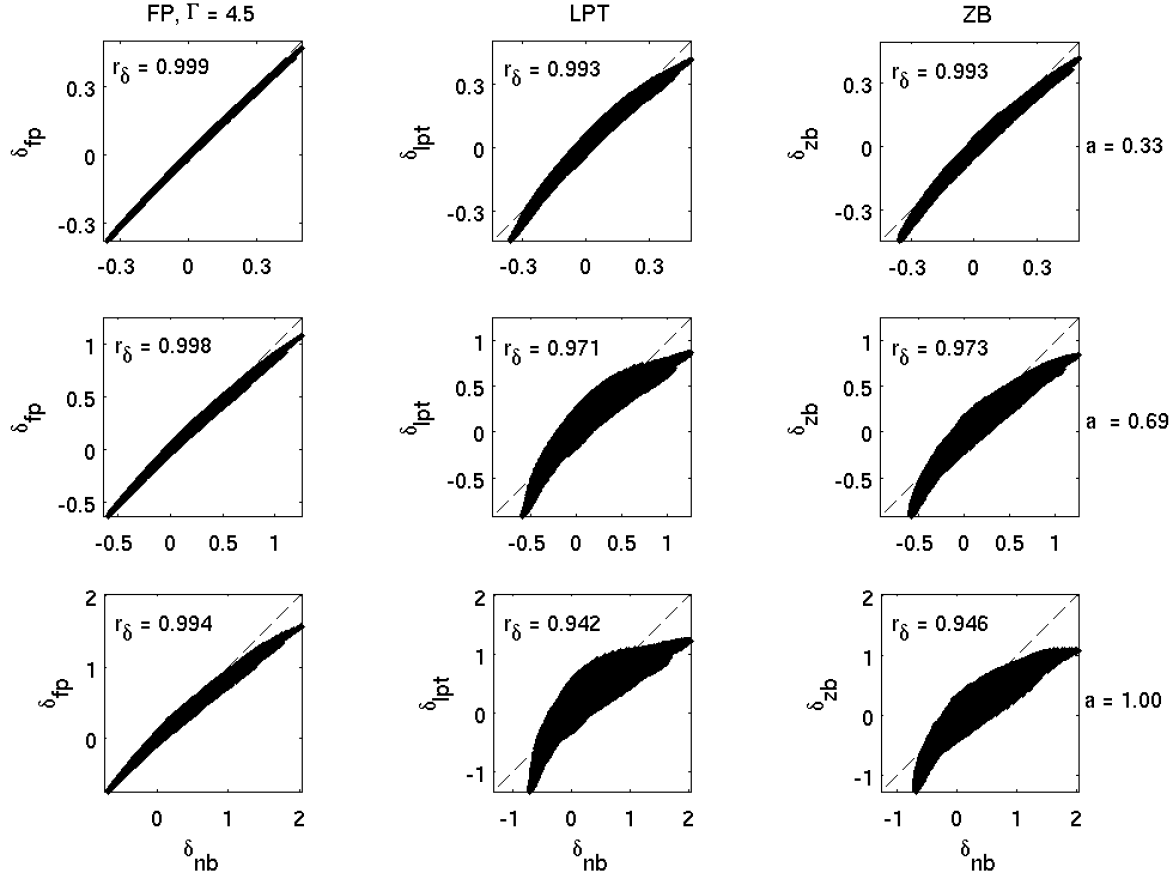


Figure 5. Point-by-point comparisons of the density fields obtained from the three approximation schemes and the N -body density field δ_{nb} . The layout of the plots is the same as in figure 4; the only difference is that all of the density fields have been smoothed with a Gaussian filter of radius $r_{sm} = 8h^{-1}$ Mpc.

Figure 5 is essentially the same as figure 4 except that all of the density fields have been smoothed with a Gaussian filter of radius $r_{sm} = 8h^{-1}$ Mpc. By using a larger smoothing scale we restrict all of the density fields to the quasi-linear regime $\delta \sim 1$. Consequently, the performance of all of the approximation methods is improved. However, the free-particle approximation still clearly out-performs the linearized fluid and Zeldovich-Bernoulli approximations. The correlation between the smoothed free-particle and N -body density fields is very good at all values of the scale factor; in particular, there is only a slight discrepancy between the two density fields in high density regions. Linear perturbation theory and the Zeldovich-Bernoulli approximation again lead (erroneously) to the formation of regions with negative density at late times.

The correlation coefficient r_δ provides a simple way of quantifying the scatter about the diagonal in the point-by-point comparisons of figure 4 and figure 5. In figure 6 we plot r_δ as a function of the scale factor for each approximation method. Results are shown for the two smoothing scales $r_{sm} = 4h^{-1}$ Mpc and $r_{sm} = 8h^{-1}$ Mpc. It is immediately

clear that, for both smoothing lengths, the free-particle approximation consistently yields a higher value of r_δ than LPT and the Zeldovich-Bernoulli approximation. It is interesting to note that, when the free-particle density field is smoothed with a Gaussian filter of radius $r_{\text{sm}} = 4h^{-1}$ Mpc, the value of r_δ obtained is always larger than that calculated from the linearized fluid and Zeldovich-Bernoulli density fields smoothed on a scale of $8h^{-1}$ Mpc. In other words, even when the linearized fluid and Zeldovich-Bernoulli density fields are more heavily smoothed than the free-particle density field, the correlation with the N -body density field is still not as good. We think this is directly attributable to the fact that the free-particle density field is guaranteed to be non-negative everywhere and so tends to provide a much better match to the N -body density field in under-dense regions.

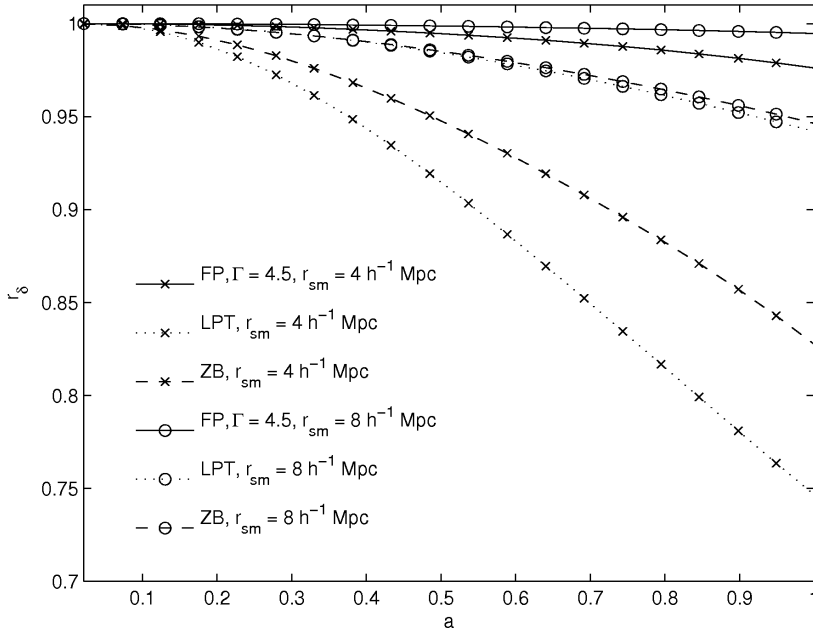


Figure 6. The correlation coefficient r_δ for each of the three approximation schemes plotted as a function of the scale factor a . Results are shown for the two smoothing lengths $r_{\text{sm}} = 4h^{-1}$ Mpc and $r_{\text{sm}} = 8h^{-1}$ Mpc.

For the sake of completeness we also investigate the behaviour of the quantum pressure term when the free-particle density field is smoothed with Gaussian filters of radii $4h^{-1}$ Mpc and $8h^{-1}$ Mpc. At each time step we use the smoothed density field to construct smoothed convective and quantum pressure terms by applying (40) and (41) respectively. We apply smoothing to the free-particle density field before calculating the quantum pressure and convective terms to ensure that any numerical gradients are well behaved. As before we then calculate the ratio $\chi = \langle |\mathcal{P}| \rangle / \langle |\mathcal{C}| \rangle$. The dashed and dotted lines in figure 3 show how χ evolves with time when $r_{\text{sm}} = 4h^{-1}$ Mpc and $r_{\text{sm}} = 8h^{-1}$ Mpc respectively. In both cases it is evident that χ is small at all times and that the value of χ decreases as the smoothing scale is made larger. This implies that, on average, the smoothed convective term dominates the smoothed quantum pressure term in (39)

and, as the smoothing scale is increased, the quantum pressure term essentially becomes negligible relative to the convective term.

A simple means of examining the statistical properties of the density fields in the different approximation schemes is afforded by the one-point probability distribution function (PDF) $P_\delta = P_\delta(\delta)$ of the density fields. The PDF of the initial N -body density field is Gaussian by construction. However, non-linear gravitational evolution causes the N -body PDF to become non-Gaussian at late times. The distribution becomes skewed since positive density fluctuations (over-densities) can grow indefinitely whereas negative density fluctuations (under-densities) cannot exceed $\delta = -1$. Figure 7 shows the PDFs of the various density fields at the present time $a_0 = 1$ for the two smoothing lengths $r_{\text{sm}} = 4h^{-1}$ Mpc and $r_{\text{sm}} = 8h^{-1}$ Mpc. The corresponding PDFs of the N -body density field are shown for reference. It is evident that, for both smoothing scales, the PDF of the free-particle density field provides the best match to the N -body PDF for all values of δ . In particular, the free-particle PDF is skewed in the same way as the PDF of the N -body density field. This is again due to the fact that $\delta \geq -1$ in the free-particle approximation. It is clear from both plots in figure 7 that the PDF of the linearized fluid density field is Gaussian. This must be the case if the initial distribution of density fluctuations was Gaussian since the density contrast at a given point simply grows proportional to the scale factor in LPT. The PDFs of the Zeldovich-Bernoulli density fields also seem to be close to Gaussian. Consequently the linearized fluid and Zeldovich-Bernoulli approximations assign a non-zero probability to the existence of regions with $\delta < -1$ at late times.

In our discussion so far we have only compared the performance of the free-particle, linearized fluid and Zeldovich-Bernoulli approximations in real space. However, it is informative to examine the behaviour of the different approximation schemes in Fourier space as well. For each method we investigate how the Fourier components $\hat{\delta} = \hat{\delta}(\mathbf{k}, a)$ of the appropriate density field evolve relative to the corresponding Fourier components $\hat{\delta}_{\text{nb}} = \hat{\delta}_{\text{nb}}(\mathbf{k}, a)$ of the N -body density field. To do this we use the statistic $\epsilon = \epsilon(k, a)$ given by

$$\epsilon = \frac{\sum |\hat{\delta} - \hat{\delta}_{\text{nb}}|^2}{\sum (|\hat{\delta}|^2 + |\hat{\delta}_{\text{nb}}|^2)}, \quad (43)$$

where, for each (comoving) wavenumber k , the summations are over all wavevectors \mathbf{k} with a magnitude in the interval $(k - \pi/L, k + \pi/L]$. The quantity ϵ provides a measure of the differences between the amplitudes and phases of the Fourier components $\hat{\delta}$ and $\hat{\delta}_{\text{nb}}$. If the amplitudes and phases of the Fourier components of the two fields are identical then $\epsilon = 0$. On the contrary, if the phases of the two fields are completely uncorrelated then $\epsilon = 1$ on average. A convenient property of the statistic ϵ is that it is independent of any smoothing of the density fields and so we are free to use the unsmoothed density fields to calculate ϵ . Figure 8 shows ϵ as a function of the wavenumber k at the present time $a_0 = 1$ for the different approximation schemes we are considering. The vertical dashed line shown in the plot denotes the wavenumber $k_{\text{nl}} = 0.3927h$

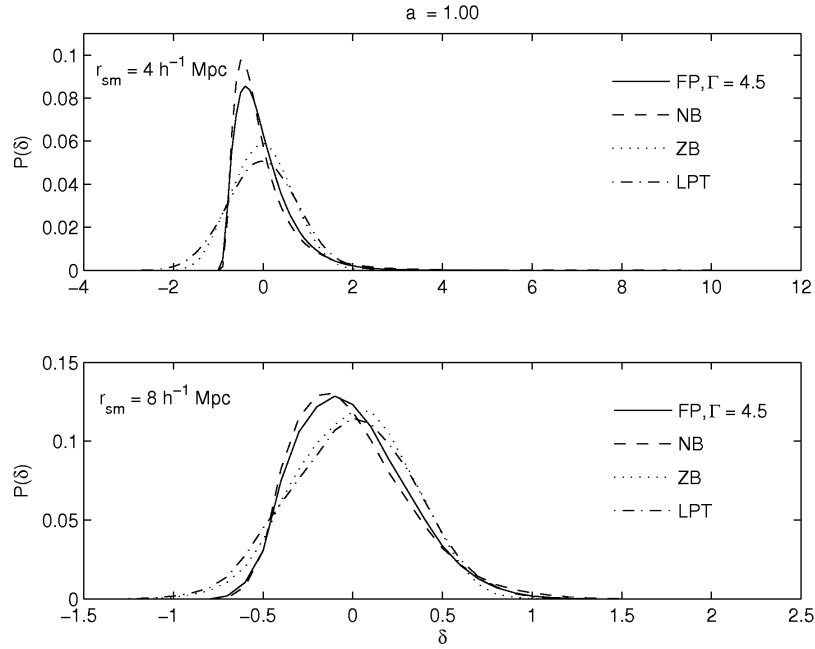


Figure 7. The one-point PDFs P_δ of the density fields obtained from the free-particle (with $\Gamma = 4.5$), linearized fluid and Zeldovich-Bernoulli approximations. The N -body PDFs are also shown for comparison. The value of the scale factor is $a = a_0 = 1$ and the top and bottom plots correspond to the smoothing lengths $r_{\text{sm}} = 4h^{-1}$ Mpc and $r_{\text{sm}} = 8h^{-1}$ Mpc respectively.

Mpc^{-1} which corresponds to a wavelength of $\lambda_{k_{\text{nl}}} = 16h^{-1}$ Mpc. From observations, the present rms density fluctuation in spheres of diameter $\lambda_{k_{\text{nl}}}$ is of order unity and so the scale k_{nl} can be taken as an indication of the boundary between modes in the linear and non-linear regimes of gravitational evolution. Fourier modes with a wavenumber $k < k_{\text{nl}}$ are still in the linear regime and evolve independently of each other. The phase information of the initial density field is preserved in this case. On the other hand, modes with a wavenumber $k \geq k_{\text{nl}}$ experience phase shifts due to coupling between different modes in the non-linear regime (Ryden and Gramman 1991, Chiang and Coles 2000). It is apparent from figure 8 that, for all of the approximation schemes, the value of ϵ becomes larger as k is increased. This is not surprising since the various methods we are comparing cannot accurately follow the non-linear evolution of small-scale modes. The main point of figure 8 is that, for wavenumbers in the range $0 < k \lesssim 3k_{\text{nl}}$, the value of ϵ is consistently smaller in the free-particle approximation than in LPT and the Zeldovich-Bernoulli approximation. In particular, the free-particle approximation performs much better than the linearized fluid and Zeldovich-Bernoulli approximations for $0 < k < k_{\text{nl}}$. Notice that the Zeldovich-Bernoulli approximation gives a slightly lower value of ϵ than the free-particle approximation for $k \gtrsim 3k_{\text{nl}}$. However, the wavenumber $k = 3k_{\text{nl}}$ corresponds to a wavelength $\lambda_{3k_{\text{nl}}} = 5.333h^{-1}$ Mpc and we find that the rms density fluctuation in spheres of diameter $\lambda_{3k_{\text{nl}}}$ is approximately 2.2 for the final N -body density field. Thus we cannot realistically expect the free-particle

and Zeldovich-Bernoulli approximations to yield reliable results on scales much smaller than this anyway.

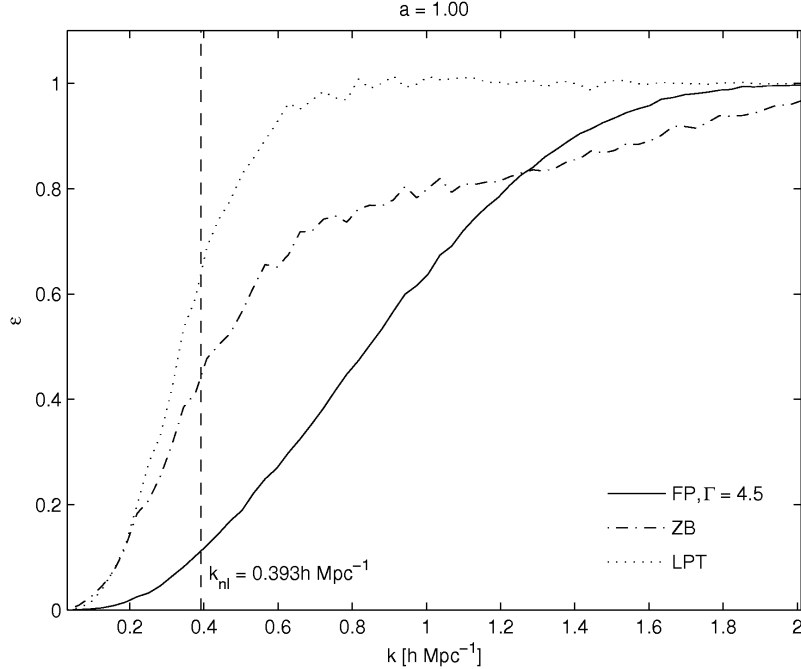


Figure 8. The statistic ϵ plotted as a function of the comoving wavenumber k for each of the three approximation schemes. The value of the scale factor is $a = a_0 = 1$. The dashed vertical line corresponds to the wavenumber $k_{nl} = 0.3927h \text{ Mpc}^{-1}$ which indicates the boundary between Fourier modes in the linear and non-linear regimes of gravitational evolution.

5. Conclusion

In this paper we have developed a new approximation method for following the gravitational evolution of initial density perturbations in a spatially-flat CDM-dominated universe. This method is based on the free-particle Schrödinger equation and is thus termed the free-particle approximation. By performing a simple transformation, the free-particle Schrödinger equation can be reduced to a system of equations that closely resembles the usual Newtonian fluid equations of motion (assuming an irrotational flow). The only difference is the presence of an extra non-linear term known as the quantum pressure term.

We have tested the free-particle approximation by appealing to a full cosmological N -body simulation. The performance of the free-particle approximation is found to be strongly dependent upon the free parameter ν (or, equivalently, the dimensionless parameter $\Gamma = \nu/\Delta^2$) appearing in the free-particle Schrödinger equation. The parameter ν controls the quantum pressure term and, as ν is increased, we find that the contribution of the quantum pressure term to the dynamics becomes more significant.

The quantum pressure term seems to inhibit the gravitational collapse of density fluctuations in the free-particle approximation. This suggests we should work in the semi-classical limit $\nu \rightarrow 0$ in order to minimize the effect of the quantum pressure term. It is in this limit that we expect to recover the usual classical fluid equations and the free-particle Schrödinger equation can be thought of as a wave-mechanical analogue of the Zeldovich approximation. However, in practice, we cannot choose ν to be arbitrarily small; there is a lower bound ν_c which is simply a consequence of the discrete grid we use to test the free-particle approximation. Therefore, we must set $\nu = \nu_c$ to ensure that the free-particle approximation gives the best possible results.

The free-particle approximation (with $\nu = \nu_c$) consistently yields better results than the established linearized fluid and Zeldovich-Bernoulli approximations in all of the tests discussed in section 4. At all times the density field obtained from the free-particle approximation is considerably better correlated with the N -body density field than the linearized fluid and Zeldovich-Bernoulli density fields. This is particularly true in low density regions which is a consequence of the fact that the free-particle density field is guaranteed to be non-negative everywhere. This feature of the free-particle approximation also explains why the one-point PDF of the free-particle density field provides the closest match to the N -body PDF of all the approximation schemes. We have also seen that the free-particle approximation out-performs LPT and the Zeldovich-Bernoulli approximation in Fourier space. From a practical point of view, another advantage of the free-particle approximation is that it is very quick to implement. This is because the free-particle Schrödinger equation has an analytic solution and so it is not necessary to numerically integrate the equations of motion as in the Zeldovich-Bernoulli approximation for example.

To conclude, we have shown that the free-particle approximation can be used to successfully follow the gravitational collapse of initial density perturbations into the quasi-linear regime, beyond the breakdown of linear perturbation theory. We have tested the free-particle approximation against two traditional approaches and the results have proved favourable. In light of these comments, we believe that the free-particle approximation provides a viable alternative to existing approaches to the study of large-scale structure formation.

Acknowledgments

C J Short would like to thank PPARC for the award of a studentship that made this work possible. Also, we are grateful to F R Pearce for many helpful comments regarding numerical issues.

Appendix A. Path integral solution of the free-particle Schrödinger equation

The solution $\psi = \psi(\mathbf{x}, a)$ to the free-particle Schrödinger equation

$$i\nu \frac{\partial \psi}{\partial a} = -\frac{\nu^2}{2} \nabla_{\mathbf{x}}^2 \psi \quad (\text{A.1})$$

can be written in the convenient form

$$\psi = \int K \psi_i d^3 \mathbf{x}', \quad (\text{A.2})$$

where $\psi_i = \psi(\mathbf{x}', a_i)$ is some initial wavefunction and $K = K(\mathbf{x}, a; \mathbf{x}', a_i)$ is the *free-particle propagator*. In the path integral formulation of quantum mechanics, the propagator involves a sum over all possible space-time paths connecting the points (\mathbf{x}', a_i) and (\mathbf{x}, a) . The path integral expression for the free-particle propagator is a standard result, see Feynman and Hibbs (1965) for example. In the case at hand the free-particle propagator is given by

$$K = \frac{1}{[2\pi i\nu(a - a_i)]^{3/2}} \exp \left[\frac{i|\mathbf{x} - \mathbf{x}'|^2}{2\nu(a - a_i)} \right], \quad (\text{A.3})$$

and so the wavefunction (A.2) becomes

$$\psi = \frac{1}{[2\pi i\nu(a - a_i)]^{3/2}} \int \exp \left[\frac{i|\mathbf{x} - \mathbf{x}'|^2}{2\nu(a - a_i)} \right] \psi_i d^3 \mathbf{x}'. \quad (\text{A.4})$$

Inserting the Madelung form

$$\psi_i = \sqrt{(1 + \delta_i)} \exp \left(\frac{-i\phi_i}{\nu} \right) \quad (\text{A.5})$$

of the initial wavefunction into (A.4) then yields

$$\psi = \frac{1}{[2\pi i\nu(a - a_i)]^{3/2}} \int \sqrt{(1 + \delta_i)} \exp \left(\frac{i}{\nu} \left[\frac{|\mathbf{x} - \mathbf{x}'|^2}{2(a - a_i)} - \phi_i \right] \right) d^3 \mathbf{x}', \quad (\text{A.6})$$

where $\delta_i = \delta(\mathbf{x}', a_i)$ is the initial density contrast field and $\phi_i = \phi(\mathbf{x}', a_i)$ is the initial comoving velocity potential. Recall that we are interested in the solution to the free-particle Schrödinger equation in the semi-classical limit $\nu \rightarrow 0$. The exponent appearing in (A.6) is complex and so the integrand will be oscillatory. Thus, in the limit $\nu \rightarrow 0$, the integrand in (A.6) will be a rapidly varying function of \mathbf{x}' . The dominant contribution to the integral in (A.6) will then be from points where the phase varies least rapidly with \mathbf{x}' , i.e. at stationary points. This method of evaluating the integral in (A.6) is known as the *method of stationary phase*. At stationary points of the phase the first derivative with respect to \mathbf{x}' vanishes leading to the condition

$$\nabla_{\mathbf{x}'} \left[\frac{|\mathbf{x} - \mathbf{x}'|^2}{2(a - a_i)} - \phi_i \right] = 0, \quad (\text{A.7})$$

and so

$$\mathbf{x} = \mathbf{x}' - (a - a_i) \nabla_{\mathbf{x}'} \phi_i. \quad (\text{A.8})$$

We now identify the initial position \mathbf{x}' with the Lagrangian coordinate \mathbf{q} and introduce a time-independent vector field $\mathbf{s} = \mathbf{s}(\mathbf{q})$ defined by $\mathbf{s} = -\nabla_{\mathbf{q}} \phi_i$. This gives rise to

$$\mathbf{x} = \mathbf{q} + (a - a_i) \mathbf{s}, \quad (\text{A.9})$$

which is simply the Zeldovich approximation in a spatially-flat CDM-dominated universe.

References

Bardeen J M 1980 *Phys. Rev. D* **22** 1882
 Bardeen J M, Bond J R, Kaiser N and Szalay A S 1986 *Astrophys. J.* **304** 15
 Brandenberger R H 1985 *Rev. Mod. Phys.* **57** 1
 Bruni M, Dunsby P K S and Ellis G F R 1992 *Astrophys. J.* **395** 34
 Chiang L Y and Coles P 2000 *Mon. Not. R. Astron. Soc.* **311** 809
 Coles P 2002 *Mon. Not. R. Astron. Soc.* **330** 421
 Coles P 2005 *Nature* **433** 248
 Coles P and Lucchin F 2002 *Cosmology: The Origin and Evolution of Cosmic Structure* (Wiley)
 Coles P, Melott A L and Shandarin S F 1993 *Mon. Not. R. Astron. Soc.* **260** 765
 Coles P and Spencer K 2003 *Mon. Not. R. Astron. Soc.* **342** 176
 Couchman H M P, Thomas P A and Pearce F R 1995 *Astrophys. J.* **452** 797
 Davies G and Widrow L M 1997 *Astrophys. J.* **485** 484
 Feynman R P and Hibbs A R 1965 *Quantum Mechanics and Path Integrals* (McGraw-Hill)
 Ghiglia D C and Pritt M D 1998 *Two-dimensional phase unwrapping: theory, algorithms and software* (Wiley)
 Hawking S W 1966 *Astrophys. J.* **145** 544
 Hockney R W and Eastwood J W 1988 *Computer Simulation Using Particles* (Institute of Physics Publishing)
 Husimi K 1940 *Proc. Phys. Math. Soc. Japan* **22** 264
 Kodama H and Sasaki M 1984 *Prog. Theor. Phys. Suppl.* **78** 1
 Kodama H and Sasaki M 1987 *Int. J. Mod. Phys. A* **2** 491
 Lifshitz E M 1946 *Sov. Phys. JETP* **10** 116
 Madelung E 1926 *Zts. f. Phys.* **40** 322
 Mukhanov V F, Feldman H A and Brandenberger R H 1992 *Phys. Rep.* **215** 203
 Nusser A and Dekel A 1992 *Astrophys. J.* **391** 443
 Peebles P J E 1980 *The Large-scale Structure of the Universe* (Princeton University Press)
 Pichon C and Bernardeau F 1999 *Astron. Astrophys.* **343** 663
 Ryden B and Gramman M 1991 *Astrophys. J.* **383** L33
 Sakurai J J 1985 *Modern Quantum Mechanics* (Benjamin/Cummings)
 Skodje R T, Rohrs H W and VanBuskirk J 1989 *Phys. Rev. A* **40** 2894
 Short C J and Coles P 2006 astro-ph/0605012
 Widrow L M and Kaiser N 1993 *Astrophys. J.* **416** L71
 Yoshisato A, Morikawa M, Gouda H and Mouri H 2006 *Astrophys. J.* **637** 555
 Zeldovich Ya B 1970 *Astron. Astrophys.* **5** 84